SOILS AND FOUNDATIONS Vol. 23, No. 2, June 1983
Japanese Society of Soil Mechanics and Foundation Engineering

SHEAR BEHAVIORS OF SAND AND CLAY UNDER THREE-DIMENSIONAL STRESS CONDITION

TERUO NAKAI* and HAJIME MATSUOKA**

ABSTRACT

The purpose of the present study is to explain the shear behaviors of soils under three-dimensional stress condition uniquely, by extending the concept of the Spatial Mobilized Plane (SMP) proposed previously. From the reconsideration of the former stress-strain model based on the SMP, new amounts of strain increments ($d\varepsilon_{SMP}$* and $d\gamma_{SMP}$*) which represent the normal and parallel components of the principal strain increment vector to the SMP are defined. Then, a new stress-strain model under shear is proposed on the basis of the idea that there exist unique relations among these new amounts of strain increments and the shear-normal stress ratio on the SMP. The validities of this stress-strain model and the failure criterion based on the SMP are confirmed using the results of the triaxial compression, triaxial extension and true triaxial tests on sand and clay. All the soil parameters of this stress-strain model can be easily determined using the conventional triaxial compression tests.

Key words : clay, dilatancy, drained shear, laboratory test, sand, shear strength, stress path, stress-strain curve (**IGC** : D 6)

INTRODUCTION

Many studies have been done concerning with the characteristics of deformation and strength of soils. However, most of them are restricted in the behaviors of soils under narrow loading conditions, and cannot explain the deformation and strength characteristics under general stress system uniquely. The authors have attempted to develope a stress-strain model for soil on the basis of "Spatial Mobilized Plane (SMP)" where soil particles are considered to be most mobilized on the average under the three-dimensional stress condition (Matsuoka and Nakai, 1974, 1977). In the present study, a new stress-strain model under shear is proposed by extending the previous model.

This paper is intended to account for the shear behaviors of sand and clay universally under the three different principal stresses. Fig. 1 shows the background of the present study, which represents a series of studies originating in the concept of the "Mobilized Plane".

* Lecturer, Department of Civil Engineering, Nagoya Institute of Technology, Gokiso-cho, Showa-ku, Nagoya.
** Associate Professor, ditto.
*** A part of the contents of the present paper was published in Japanese (Nakai and Matsuoka, 1980).
Manuscript was received for review on May 19, 1982.
Written discussions on this paper should be submitted before April 1, 1984.

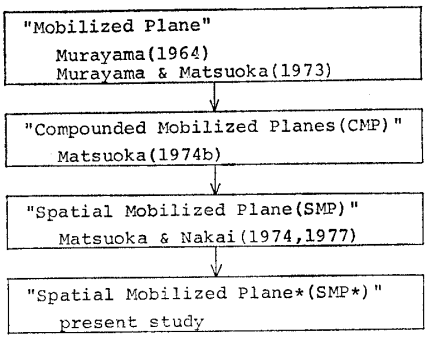

Fig. 1. Background of present study

(1) "Mobilized Plane"

In the case that three different principal stresses (σ_1, σ_2 and σ_3) are applied, three Mohr's stress circles are drawn as shown in Fig. 2. The point at which a straight line from the origin is tangent to the largest one of these stress circles represents the stress condition on the plane where the shear-normal stress ratio (τ/σ_N) is maximized. This plane has hitherto been called the "Mobilized Plane" or the "Plane of maximum mobilization" (Murayama, 1964) and considered to be a plane on which soil particles are most mobilized, because the behavior of soil particles under shear is governed by the frictional law, i. e., the shear-normal stress ratio. In the three-dimensional space where the coordinate axes I, II and III indicate the direction of the major, intermediate and minor principal stresses (σ_1, σ_2 and σ_3), respectively, the "Mobilized Plane" is represented as the plane AC in Fig. 3, which makes an angle of $(45°+\phi_{mo13}/2)$ to the III-axis and is parallel to the II-axis. The stress-strain equations for soil based on the concept of the "Mobilized Plane" (Murayama, 1964; Murayama and Matsuoka, 1973) have been derived by supposing that there exist basic relationships among the shear-normal stress ratio and the normal and shear strain increments on that plane. However, the analytical soil behaviors expressed by these equations are independent of the intermediate principal stress σ_2, since the "Mobilized Plane" is governed only by σ_1 and σ_3.

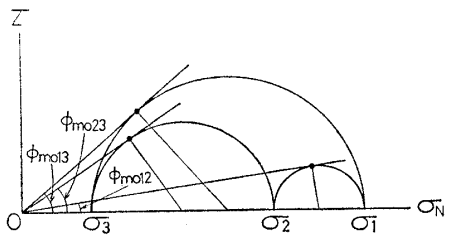

Fig. 2. Three mobilized planes where shear-normal stress ratio is maximized under respective two principal stresses

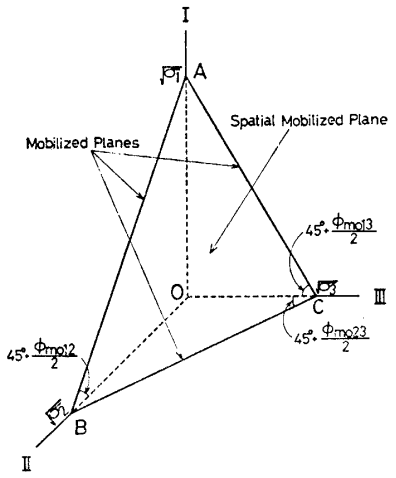

Fig. 3. Three mobilized planes and Spatial Mobilized Plane in three-dimensional space

(2) "Compounded Mobilized Planes (CMP)"

In order to consider the effect of the intermediate principal stress, one of the authors, Matsuoka (1974 b), introduced a concept of three mobilized planes (the planes AC, AB and BC in Fig. 3) by taking note of the points at which three straight lines from the origin are tangent to the three Mohr's stress circles in Fig. 2. These three mobilized planes on which the shear-normal stress ratios are maximized between the respective two axes (I-II, II-III and I-III), have generically been named the "Compounded Mobilized Planes (CMP)". Under the three-dimensional stress condition, each of three principal strains is assumed to be represented as the algebraic summation of two components produced on the corresponding two mobilized planes.

(3) "Spatial Mobilized Plane (SMP)"

Paying further attention to the plane ABC with these three mobilized planes as the three sides, the authors have defined it

as the "Spatial Mobilized Plane (SMP)" (Matsuoka and Nakai, 1974, 1977). The values at the points at which the SMP intersects the three coordinate axes are proportional to the square roots of the respective principal stresses according to the following equation

$$\tan\left(45°+\frac{\phi_{moij}}{2}\right)=\sqrt{\frac{1+\sin\phi_{moij}}{1-\sin\phi_{moij}}}=\sqrt{\frac{\sigma_i}{\sigma_j}} \quad (i,j=1,2,3\ ;\ i\geqq j) \qquad (1)$$

as shown in Fig. 3. Therefore, the SMP coincides with the octahedral plane in an isotropic stress condition and is variable with possible changes in the stresses. The direction cosines (a_1, a_2 and a_3) of the normal of the SMP are expressed as follows:

$$a_i=\sqrt{\frac{J_3}{\sigma_i\cdot J_2}} \quad (i=1,2,3) \qquad (2)$$

where J_1, J_2 and J_3 are the first, second and third effective stress invariants and are expressed by the following equations.

$$\begin{aligned} J_1&=\sigma_1+\sigma_2+\sigma_3\\ J_2&=\sigma_1\sigma_2+\sigma_2\sigma_3+\sigma_3\sigma_1\\ J_3&=\sigma_1\sigma_2\sigma_3 \end{aligned} \qquad (3)$$

A stress-strain model under the three-dimensional stress condition has been obtained based on the idea that there exist unique relations among the shear-normal stress ratio on the SMP (τ_{SMP}/σ_{SMP}) and the normal and shear strain increments on the SMP ($d\varepsilon_{SMP}$ and $d\gamma_{SMP}$), because the SMP is considered to be the plane where soil particles are most mobilized on the average in the three-dimensional space.

(4) "Spatial Mobilized Plane* (SMP*)"

The stress-strain model proposed here are derived by extending the above model based on the SMP. The details of this model will be discussed in the following section, and were described in the previous paper in Japanese (Nakai and Matsuoka, 1980).

Throughout this paper, the term "stress" is to be interpreted as "effective stress".

NEW STRESS-STRAIN MODEL UNDER SHEAR BASED ON THE SMP

A stress-strain model for soil under shear has already been proposed on the basis of the idea that there exist unique relations among the shear-normal stress ratio on the SMP (τ_{SMP}/σ_{SMP}) and the normal and shear strain increments on the SMP ($d\varepsilon_{SMP}$ and $d\gamma_{SMP}$). This model can explain various experimental results of shear tests (Matsuoka and Nakai, 1974, 1977). However, strictly investigated, there are some differences with a trend between experimental results and calculated values using this model. Therefore, in this section, considering the derivation process of this model, a new stress-strain model is proposed by introducing new amounts of strain increments based on the SMP.

Fig. 4 shows a cubical soil element and the Spatial Mobilized Plane (SMP) in the three-dimensional space, where I, II and III axes represent the directions to which three principal stresses σ_1, σ_2 and σ_3 are applied, respectively. The normal stress on the SMP (σ_{SMP}), the shear stress (τ_{SMP}) and the shear-normal stress ratio (τ_{SMP}/σ_{SMP}) are expressed as follows using Eq. (2).

$$\sigma_{SMP}=\sigma_1a_1^2+\sigma_2a_2^2+\sigma_3a_3^2=3\frac{J_3}{J_2} \qquad (4)$$

$$\begin{aligned}\tau_{SMP}&=\sqrt{(\sigma_1-\sigma_2)^2a_1^2a_2^2+(\sigma_2-\sigma_3)^2a_2^2a_3^2+(\sigma_3-\sigma_1)^2a_3^2a_1^2}\\ &=\frac{\sqrt{J_1J_2J_3-9J_3^2}}{J_2}\end{aligned} \qquad (5)$$

$$\frac{\tau_{SMP}}{\sigma_{SMP}}=\sqrt{\frac{J_1J_2-9J_3}{9J_3}} \qquad (6)$$

If the direction of the principal stresses and that of the principal strain increments are

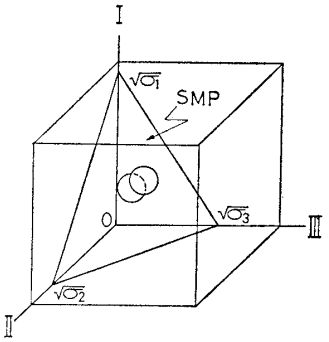

Fig. 4. Soil element and Spatial Mobilized Plane in three-dimensional space

assumed to be identical, the normal and shear strain increments on the SMP ($d\varepsilon_{SMP}$ and $d\gamma_{SMP}$) are expressed by the following equations.

$$d\varepsilon_{SMP}=d\varepsilon_1 a_1{}^2+d\varepsilon_2 a_2{}^2+d\varepsilon_3 a_3{}^2 \tag{7}$$

$$\frac{d\gamma_{SMP}}{2}=\sqrt{\begin{aligned}&(d\varepsilon_1-d\varepsilon_2)^2 a_1{}^2 a_2{}^2+(d\varepsilon_2-d\varepsilon_3)^2 a_2{}^2 a_3{}^2\\&+(d\varepsilon_3-d\varepsilon_1)^2 a_3{}^2 a_1{}^2\end{aligned}} \tag{8}$$

It has been considered that the SMP is the plane where soil particles are most mobilized on the average, and the shear-normal stress ratio on the SMP (τ_{SMP}/σ_{SMP}) governs the sliding of soil particles in the three-dimensional space, as mentioned before. According to the former stress-strain model (Matsuoka and Nakai, 1974, 1977), τ_{SMP}/σ_{SMP} has been ralated to the normal and shear strain increments on the SMP ($d\varepsilon_{SMP}$ and $d\gamma_{SMP}$), because the average sliding direction of soil particles has been considered to coincide with the direction of the strain increment vector on the SMP. However, it has become clear that the average sliding direction of soil particles coincides with the direction of the principal strain increment vector in the strict sense (see Appendix). Therefore, it is rather reasonable not to use the normal and shear strain increment on the SMP ($d\varepsilon_{SMP}$ and $d\gamma_{SMP}$) but to use the normal and parallel components of the principal strain increment vector to the SMP ($d\varepsilon_{SMP}{}^*$ and $d\gamma_{SMP}{}^*$). Fig. 5 indicates the principal strain increment space, in which the principal strain increment vector $\overrightarrow{d\varepsilon_i}=(d\varepsilon_1,\ d\varepsilon_2,\ d\varepsilon_3)$ is denoted by the vector $\overrightarrow{OP}$. On the assumption that the direction of the principal stresses and that of the principal strain increments are identical, $d\varepsilon_{SMP}{}^*$ and $d\gamma_{SMP}{}^*$, which denote the normal component $\overrightarrow{ON}$ and the parallel component $\overrightarrow{NP}$ of the vector $\overrightarrow{OP}$ to the SMP respectively, can be expressed by the following equation.

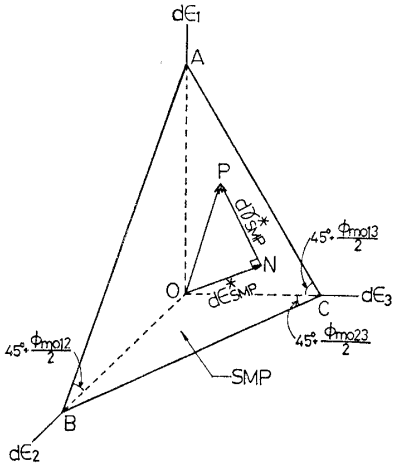

Fig. 5. Amounts of strain increments ($d\varepsilon_{SMP}{}^*$ and $d\gamma_{SMP}{}^*$) in principal strain increment space

$$d\varepsilon_{SMP}{}^*=d\varepsilon_1 a_1+d\varepsilon_2 a_2+d\varepsilon_3 a_3 \tag{9}$$

$$d\gamma_{SMP}{}^*=\sqrt{\begin{aligned}&(d\varepsilon_1 a_2-d\varepsilon_2 a_1)^2+(d\varepsilon_2 a_3-d\varepsilon_3 a_2)^2\\&+(d\varepsilon_3 a_1-d\varepsilon_1 a_3)^2\end{aligned}} \tag{10}$$

In the present study, by introducing the new amounts of strain increments based on the SMP ($d\varepsilon_{SMP}{}^*$ and $d\gamma_{SMP}{}^*$) defined by Eqs. (9) and (10) instead of ($d\varepsilon_{SMP}$ and $d\gamma_{SMP}$) in Eqs. (7) and (8), a new stress-strain model under shear is derived.

Now, if the basic equations on the mobilized plane derived by Matsuoka (1974 a, 1974 b) are assumed to hold among τ_{SMP}/σ_{SMP}, $d\varepsilon_{SMP}{}^*$ and $d\gamma_{SMP}{}^*$ in the same manner as among τ_{SMP}/σ_{SMP}, $d\varepsilon_{SMP}$ and $d\gamma_{SMP}$ in the former model, the following equations can be obtained.

$$\frac{\tau_{SMP}}{\sigma_{SMP}}=\lambda^*\cdot\left(-\frac{d\varepsilon_{SMP}{}^*}{d\gamma_{SMP}{}^*}\right)+\mu^* \tag{11}$$

$$\frac{\tau_{SMP}}{\sigma_{SMP}}=\lambda^*\cdot\left(-\frac{\varepsilon_{SMP}{}^*}{\gamma_{SMP}{}^*}\right)+\mu'^* \tag{12}$$

$$\left(\varepsilon_{SMP}{}^*=\int d\varepsilon_{SMP}{}^* \text{ and } \gamma_{SMP}{}^*=\int d\gamma_{SMP}{}^*\right)$$

where λ^*, μ^* and μ'^* are the soil parameters. By solving the differential equation obtained from Eqs. (11) and (12), the following equation is derived.

$$\gamma_{SMP}{}^*=\gamma_o{}^*\cdot\exp\left(\frac{X-\mu^*}{\mu'^*-\mu^*}\right) \tag{13}$$

where X represents τ_{SMP}/σ_{SMP} and $\gamma_o{}^*$ is the soil parameter. From Eqs. (11) and (13), $d\gamma_{SMP}{}^*$ and $d\varepsilon_{SMP}{}^*$ are given as functions of the stress ratio.

$$d\gamma_{SMP}{}^*=\frac{\gamma_o{}^*}{\mu'^*-\mu^*}\cdot\exp\left(\frac{X-\mu^*}{\mu'^*-\mu^*}\right)\cdot dX \tag{14}$$

$$d\varepsilon_{SMP}^* = \frac{\mu^* - X}{\lambda^*} \cdot d\gamma_{SMP}^* \quad (15)$$

$$(X \equiv \tau_{SMP}/\sigma_{SMP})$$

The soil parameters (λ^*, μ^*, μ'^* and γ_o^*) in Eqs. (14) and (15) have the same properties as those (λ, μ, μ' and γ_o) in the former stress-strain model. Each of the parameters λ^*, μ^* and μ'^* is considered to be nearly constant for a given sample. On the other hand, γ_o^* is affected by the initial soil structure and the confining stress, and is empirically expressed by the following formula using the mean principal stress σ_m in the case that the initial structures of samples are similar.

$$\gamma_o^* = \gamma_{oi}^* + C_d^* \cdot \log_{10} \frac{\sigma_m}{\sigma_{mi}} \quad (16)$$

where σ_{mi} is the basic value of σ_m, γ_{oi}^* is the value of γ_o^* at $\sigma_m = \sigma_{mi}$, and C_d^* is a coefficient determined by the sample and its initial structure.

The direction cosines of $d\varepsilon_{SMP}^*$ are equal to a_i ($i=1, 2, 3$) given by Eq. (2), on the assumption that the direction of the principal stresses and that of the principal strain increments are identical. If it is assumed that the parallel component of the average sliding of soil particles to the SMP coincides with τ_{SMP} in direction, the direction cosines of $d\gamma_{SMP}^*$ are expressed by the following direction cosines of τ_{SMP}.

$$b_i = \frac{\sigma_i - \sigma_{SMP}}{\tau_{SMP}} \cdot a_i = \frac{\sigma_i J_2 - 3J_3}{\sqrt{\sigma_i J_2 (J_1 J_2 - 9J_3)}} \quad (17)$$

$$(i=1, 2, 3)$$

Accordingly, the principal strain increments $d\varepsilon_i$ ($i=1, 2, 3$) can be calculated from $d\varepsilon_{SMP}^*$ and $d\gamma_{SMP}^*$ using the following formula.

$$d\varepsilon_i = a_i \cdot d\varepsilon_{SMP}^* + b_i \cdot d\gamma_{SMP}^*$$
$$= \sqrt{\frac{J_3}{\sigma_i J_2}} \cdot d\varepsilon_{SMP}^* + \frac{\sigma_i J_2 - 3J_3}{\sqrt{\sigma_i J_2 (J_1 J_2 - 9J_3)}} d\gamma_{SMP}^* \quad (i=1, 2, 3) \quad (18)$$

Substituting Eqs. (14) and (15) into Eq. (18), the principal strain increments due to shear are obtained as the function of stresses and the soil parameters.

SPECIMENS, APPARATUS AND TEST PROCEDURE

Sand

The saturated Toyoura sand was used in this investigation. The mean diameter of the sand is 0.2 mm, the uniformity coefficient is 1.3 and the specific gravity is 2.65. The maximum and minimum void ratios of the sand are 0.95 and 0.58, respectively. Specimens were prepared by pouring the saturated sand into a mold in several layers and compacting each layer with the rod whose diameter was 6 mm so that the specimens had a desired initial void ratio ($e_0 \simeq 0.68$). It was checked using isotropic consolidation tests that the specimens prepared in this manner had an isotropic initial structure. In addition to the above specimens, the loose specimens ($e_0 \simeq 0.80$) and the anisotropic specimens ($e_0 \simeq 0.68$) were also used partially in this paper.

The tests on sand were the triaxial compression and triaxial extension tests using cylindrical specimens, and the true triaxial tests using rectangular specimens.

(1) Triaxial compression and Triaxial extension tests

Triaxial compression ($\sigma_1 > \sigma_2 = \sigma_3$) and triaxial extension ($\sigma_1 = \sigma_2 > \sigma_3$) tests were carried out by employing the stress-controlled triaxial test apparatus in which axial and lateral stresses were applied independently to the specimen with 5 cm in diameter and 12 cm in height.

(2) True triaxial tests

True triaxial tests ($\sigma_1 \geqq \sigma_2 \geqq \sigma_3$) were carried out by such type of true triaxial test apparatus as shown in Photo. 1, which permitted application of three different principal stresses to a specimen of 5 cm × 5 cm × 10 cm in size. One of two horizontal stresses was applied by the chamber pressure, and the other by a couple of rubber pressure bags through the stiff plates suspended by the rubber bands or the coil springs, as shown in Fig. 6. A vertical stress was transmitted by a piston through the stiff plate. In the present investigation, the accuracy of the

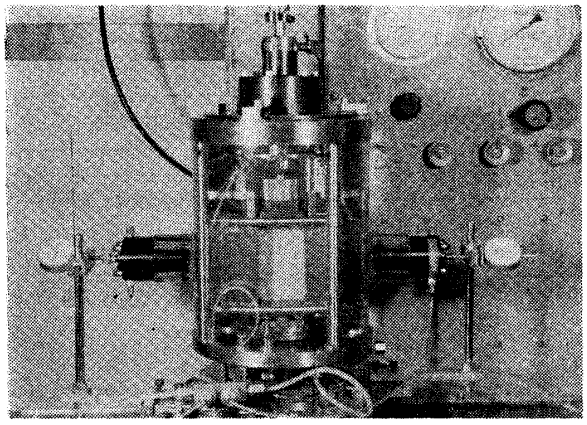

Photo. 1. Whole view of true triaxial test apparatus

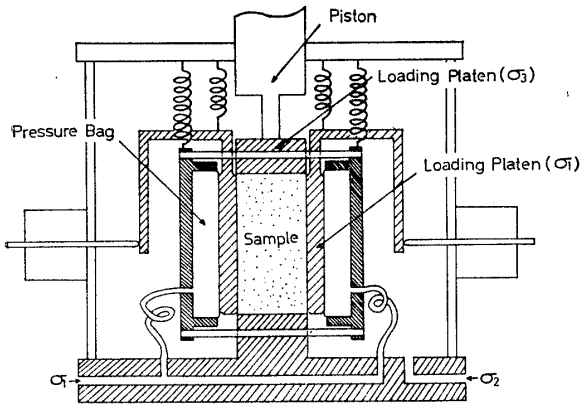

Fig. 6. Sketch of true triaxial test apparatus

test was improved by contriving the method of loading in the following way. The major principal stress σ_1 was applied by the pressure bags in the chamber, the intermediate principal stress σ_2 by the chamber pressure and the minor principal stress σ_3 by the piston at the top of the chamber. Therefore, the effect of arching at the corners of specimen, which was one of the shortcomings in such type of apparatus, could be made small, because when the horizontal loading plates in the direction of σ_1 moved toward the specimen, the other vertical loading plate in the direction of σ_3 moved outward. Moreover, the horizontal loading plates and pressure bags were floated by the rubber bands or the springs in the chamber so as to reduce the effect of friction to the specimen.

The friction between the specimen and the

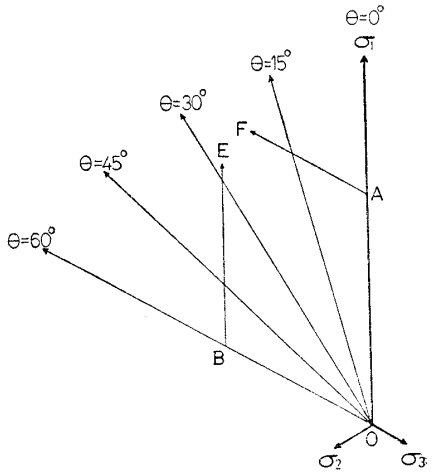

Fig. 7. Stress paths on octahedral plane for true triaxial test

loading plate was also reduced by the rubber membranes and Teflon sheets coated with silicon grease. All the tests were carried out by means of stress-controlled method under the drained condition.

In soil mechanics, the deformation of soil caused by the change in stress ratio under a constant mean principal stress is ordinarily considered to be the deformation due to shear. All of the triaxial compression, triaxial extension tests and true triaxial tests were performed under constant mean principal stresses. Fig. 7 shows the stress paths for true triaxial tests on the octahedral plane (mean principal stress $\sigma_m=196\,\mathrm{kN/m^2}$). As shown in Fig. 7, the radial stress paths are named $\theta=0°$, 15°, 30°, 45° and 60° after the angle of θ between the σ_1-axis and the respective radial stress paths on the octahedral plane. $\theta=0°$ and $\theta=60°$ corresponds to the triaxial compression and triaxial extension conditions, respectively. The following relationship exists among the angle of radial stress path θ and the principal stresses (σ_1, σ_2 and σ_3).

$$\tan\theta=\sqrt{3}\frac{(\sigma_2-\sigma_3)}{(\sigma_1-\sigma_2)+(\sigma_1-\sigma_3)} \qquad (19)$$

The path O-A-F indicates that the stress point moves to $\sigma_1/\sigma_3=3$ along the straight path $\theta=0°$ and turns its direction for 60° as illustrated in the figure. The stress point of the path O-B-E moves to $\sigma_1/\sigma_3=3$ along

$\theta=60°$ and turns its direction for $-60°$.

Clay

The specimen used in the tests are called the Fujinomori clay (the liquid limit $w_L=44.7\%$, the plastic limit $w_p=24.7\%$ and the specific gravity $G_s=2.65$) and prepared as follows. The powdered Fujinomori clay was thoroughly mixed with water at a water content of about 80%, and then the mixed clay was consolidated one-dimensionally under a pressure of 49 kN/m². The specimens were formed in the shape of cylinders of 3.5 cm in diameter and 8 cm in height. The initial water content of the specimens was nearly 40%.

The triaxial compression and triaxial extension tests were carried out using the conventional triaxial test apparatus. The slotted filter paper on the circumference of the specimen was not employed in the tests so as to avoid the effect of tension of the paper, though it was ordinarily used. Therefore, the drainage of the specimen was allowable only at the top and bottom of the specimen. All the tests were carried out by means of strain-controlled method under the drained condition at a speed of the axial strain rate $\dot{\varepsilon}_a=5.5\times10^{-4}\%$/min which is a sufficiently low speed for the drained tests. The tests were performed under a constant mean principal stress in the same manner as the tests on sand.

EXPERIMENTAL ASSESSMENTS

Sand

The sand specimen used here implies the above isotropic medium dense sand ($e_0\simeq 0.68$), if there is no special explanation about specimen. Fig. 8 shows the results of the triaxial compression and triaxial extension tests on the sand with respect to the relation between τ_{SMP}/σ_{SMP} and $d\varepsilon_{SMP}^*/d\gamma_{SMP}^*$ in Eq. (11) (mean principal stresses $\sigma_m=196$ kN/m² and 392 kN/m²). Figs. 9 and 10 indicate the results of the true triaxial tests on the sand ($\sigma_m=196$ kN/m²). From these figures it can be seen that all the test results are

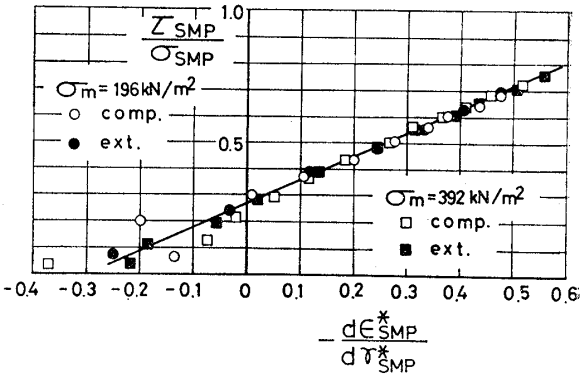

Fig. 8. Relation between τ_{SMP}/σ_{SMP} and $d\varepsilon_{SMP}^*/d\gamma_{SMP}^*$ obtained by triaxial compression and triaxial extension tests on sand

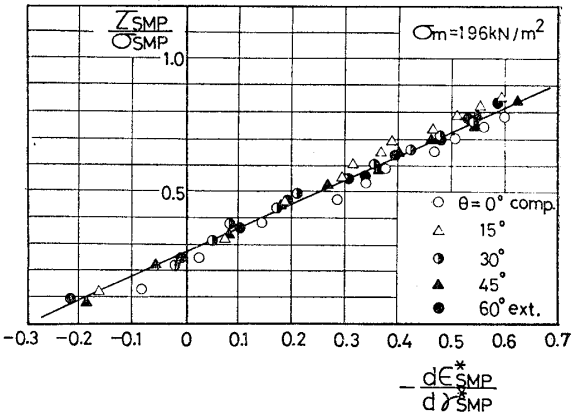

Fig. 9. Relation between τ_{SMP}/σ_{SMP} and $d\varepsilon_{SMP}^*/d\gamma_{SMP}^*$ obtained by true triaxial tests (stress path : θ=const.) on sand

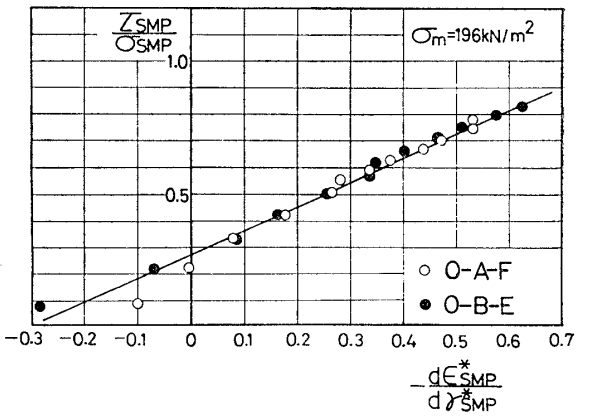

Fig. 10. Relation between τ_{SMP}/σ_{SMP} and $d\varepsilon_{SMP}^*/d\gamma_{SMP}^*$ obtained by true triaxial test (stress path : O-A-F and O-B-E) on sand

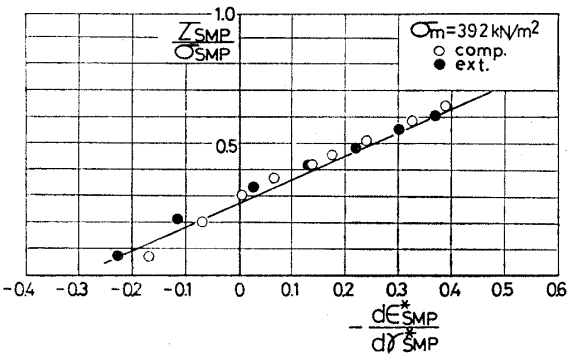

Fig. 11. Relation between τ_{SMP}/σ_{SMP} and $d\varepsilon_{SMP}^*/d\gamma_{SMP}^*$ obtained by triaxial compression and triaxial extension tests on loose sand ($e_0 \simeq 0.80$)

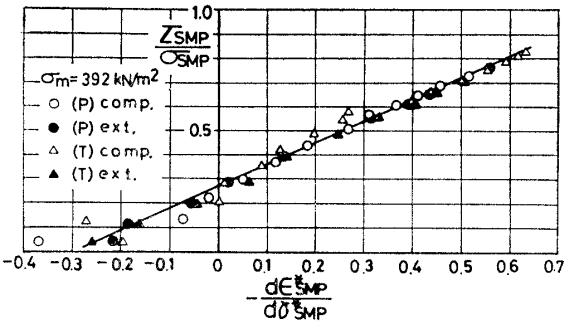

Fig. 12. Relation between τ_{SMP}/σ_{SMP} and $d\varepsilon_{SMP}^*/d\gamma_{SMP}^*$ obtained by triaxial compression and triaxial extension tests on isotropic and anisotropic sand

arranged on a unique linear line in spite of the magnitude of mean principal stresses and the change of stress paths, and Eq. (11) has a good estimate. The soil parameters of the sand λ^* and μ^* can be determined as $\lambda^*=0.9$ and $\mu^*=0.27$ from the values of linear gradient and ordinate intercept of the lines in these diagram. Fig. 11 indicates the results of the triaxial compression and triaxial extension tests on the loose sand ($e_0 \simeq 0.80$) in the same arrangement as above. Fig. 12 shows the results of the triaxial compression and triaxial extension tests on the isotropic sand and the anisotropic sands. In this figure, the open and solid circles represent the isotropic sand which is the same as indicated in Fig. 8, and the open and solid triangles represent the anisotropic sand in which sand particles are arranged horizontally.

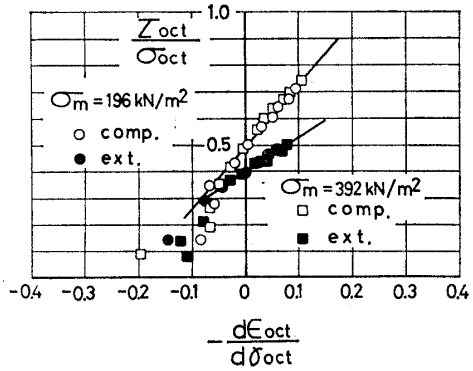

Fig. 13. Relation between τ_{oct}/σ_{oct} and $d\varepsilon_{oct}/d\gamma_{oct}$ obtained by same tests as Fig. 8

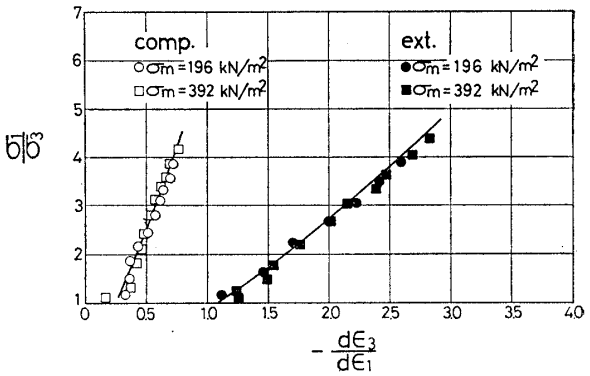

Fig. 14. Relation between σ_1/σ_3 and $d\varepsilon_3/d\varepsilon_1$ obtained by same tests as Fig. 8

As can be seen from these figures, Eq. (11) is affected by neither the void ratio nor the initial structure of sand. Fig. 13 shows the results of the same tests as in Fig. 8, arranged with respect to the relation between the shear-normal stress ratio on the octahedral plane (τ_{oct}/σ_{oct}) and the normal-shear strain increment ratio on the octahedral plane ($d\varepsilon_{oct}/d\gamma_{oct}$). Roscoe et al. have derived the following relationship between stress ratio and strain increment ratio using the equation of energy dissipation (Roscoe et al, 1963; Schofield and Wroth, 1968).

$$\frac{\tau_{oct}}{\sigma_{oct}}=\frac{\sqrt{2}}{3}M-2\frac{d\varepsilon_{oct}}{d\gamma_{oct}} \qquad (20)$$

However, it is not seen in Fig. 13 that the results of triaxial compression and triaxial extension tests are arranged on an unique line. Fig. 14 shows the results of the same tests as in Fig. 8 with plots, and the theoretical values derived from Eq. (11) with solid

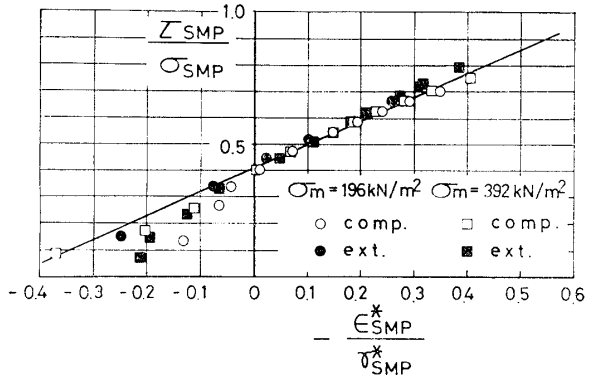

Fig. 15. Relation between τ_{SMP}/σ_{SMP} and $\varepsilon_{SMP}^*/\gamma_{SMP}^*$ obtained by same triaxial compression and triaxial extension tests as Fig. 8

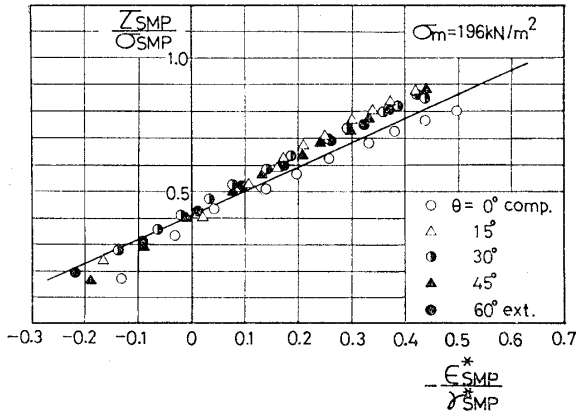

Fig. 16. Relation between τ_{SMP}/σ_{SMP} and $\varepsilon_{SMP}^*/\gamma_{SMP}^*$ obtained by same true triaxial tests as Fig. 9

lines, with respect to the relation between the principal stress ratio (σ_1/σ_3) and the principal strain increment ratio $(d\varepsilon_3/d\varepsilon_1)$ according to the Rowe's stress-dilatancy equation (Rowe, 1962). The theoretical values explain well the difference of the observed dilatancy characteristics between the triaxial compression and triaxial extension conditions.

Fig. 15 indicates the results of the same triaxial compression and triaxial extension tests as shown in Fig. 8, with respect to the relation between τ_{SMP}/σ_{SMP} and $\varepsilon_{SMP}^*/\gamma_{SMP}^*$ in Eq. (12). Fig. 16 shows the results of the same true triaxial tests as shown in Fig. 9. It is observed from these figures that Eq. (12) as well as Eq. (11) holds uniquely regardless of the stress paths on the octahedral plane. The soil parameter μ'^* in Eq.

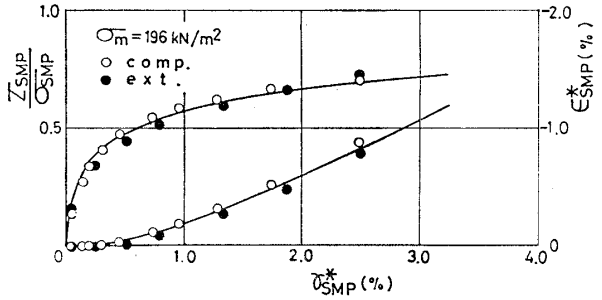

Fig. 17. Relation among τ_{SMP}/σ_{SMP}, γ_{SMP}^* and ε_{SMP}^* obtained by triaxial compression and triaxial extension tests (σ_m=196 kN/m²) on sand

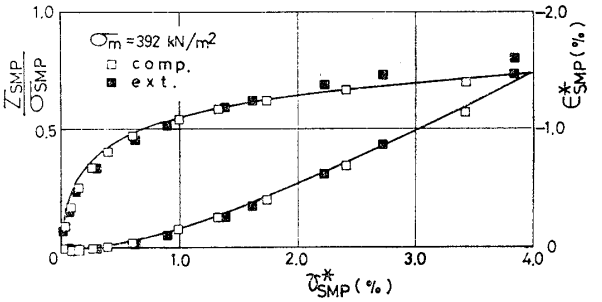

Fig. 18. Relation among τ_{SMP}/σ_{SMP}, γ_{SMP}^* and ε_{SMP}^* obtained by triaxial compression and triaxial extension tests (σ_m=392 kN/m²) on sand

(12) can be determined as $\mu'^*=0.41$.

Figs. 17 and 18 show the relation among τ_{SMP}/σ_{SMP}, γ_{SMP}^* and ε_{SMP}^* obtained from the triaxial compression and triaxial extension tests under constant mean principal stresses σ_m=196 kN/m² and 392 kN/m², respectively. The plots represent the observed values and the solid curves the values calculated using Eqs. (14) and (15). λ^*, μ^* and μ'^* of the soil parameters are determined from the arrangements in Figs. 8 and 15 as mentioned before. The parameters γ_{oi}^* and C_d^* related to γ_o^* are determined from the arrangement of the relationship between γ_o^* and $\log_{10}\sigma_m$ obtained by more than two tests under different mean principal stresses. All the soil parameters of the sand are listed in Table 1. Fig. 19 indicates the results of the true triaxial tests (θ=0°, 15°, 30°, 45° and 60°) in the same manner as in Figs. 17 and 18. It is seen in this figure that regardless of the stress paths the observed values are

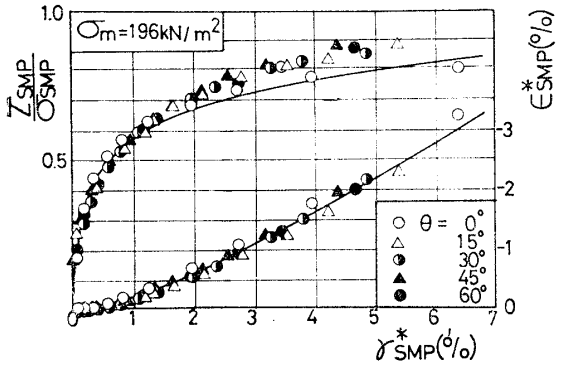

Fig. 19. Relation among τ_{SMP}/σ_{SMP}, $\gamma_{SMP}{}^*$ and $\varepsilon_{SMP}{}^*$ obtained by true triaxial tests on sand

Table 1. Values of all soil parameters for sand

λ^*		0.9
μ^*		0.27
μ'^*		0.41
$\gamma_o{}^*$	$\gamma_{oi}{}^*$	0.10%
	$C_d{}^*$	0.066%
	σ_{mi}	98 kN/m²

plotted nearly on the same curves calculated using the soil parameters in Table 1. Fig. 20 shows the results of the same tests as shown in Fig. 18 in terms of the relation among τ_{oct}/σ_{oct}, γ_{oct} and ε_{oct}. The test data arranged on the octahedral plane vary from the triaxial compression to the triaxial extension conditions with a trend in the same way as shown in Fig. 13, while the results are uniquely analyzed in the case of Fig. 18.

Fig. 21 shows the observed values and the calculated curves for the triaxial compression and triaxial extension tests under a constant mean principal stress $\sigma_m=392\,kN/m^2$, as plotted in terms of the relation among the principal stress ratio (σ_1/σ_3) and the principal strains $(\varepsilon_1$ and $\varepsilon_3)$. Fig. 22 indicates the results of the same test and the calculated curves with respect to the relation between the stress ratio (σ_1/σ_3) and the volumetric strain (ε_v). In these figures, the solid curves represent the calculated values under the triaxial compression condition, and the broken curves with dots express those under the triaxial extension condition. These calculated values are obtained from Eqs. (14), (15) and (18) using the soil parameter in Table 1 determined by two triaxial compression tests under different mean principal stresses as mentioned before. It is seen in Fig. 22 that the proposed stress-strain model

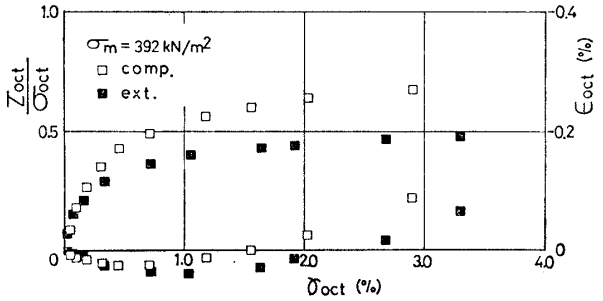

Fig. 20. Relation among τ_{oct}/σ_{oct}, γ_{oct} and ε_{oct} obtained by same tests as Fig. 18

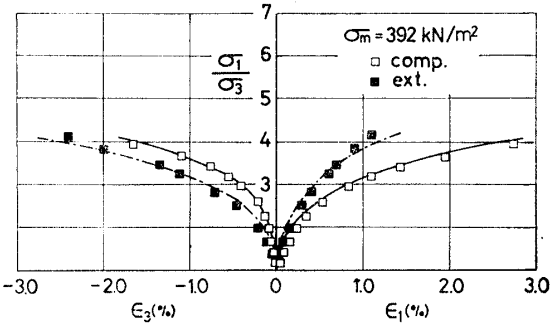

Fig. 21. Principal stress ratio vs. principal strains in triaxial compression and triaxial extention tests ($\sigma_m=392\,kN/m^2$) on sand

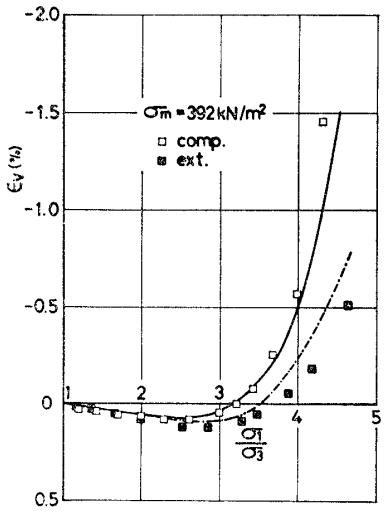

Fig. 22. Volumetric strain vs. principal stress ratio in same tests as Fig. 21

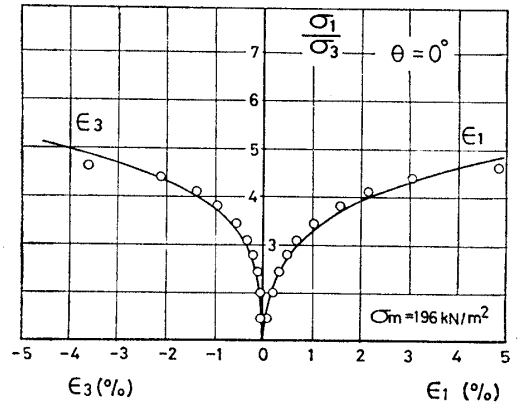

(a)

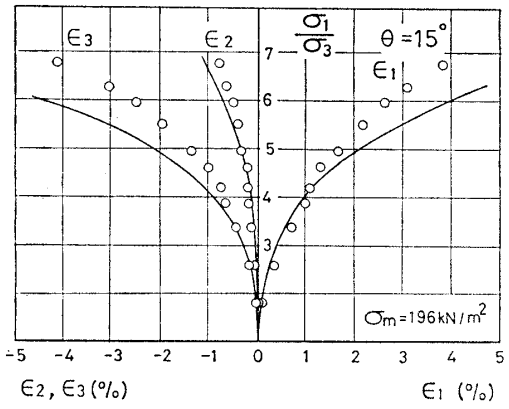

(b)

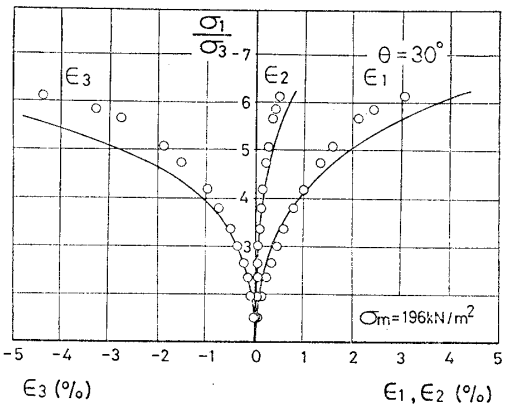

(c)

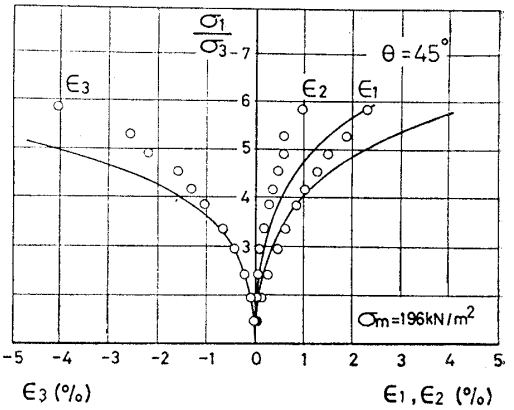

(d)

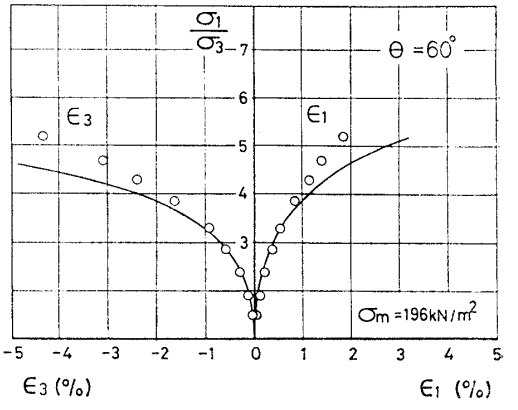

(e)

Fig. 23. Principal stress ratio vs. principal strains in true triaxial tests (θ=0°, 15°, 30°, 45° and 60°) on sand

explains well the dilatancy characteristics of sand under the triaxial compression and triaxial extension conditions. The former stress-strain model based on the SMP (Matsuoka and Nakai, 1974, 1977), however, did not explain such a difference of the observed values between the triaxial compression and triaxial extension conditions illustrated in this figure. Figs. 23(a)-(e) show the results of the true triaxial tests (θ=0°, 15°, 30°, 45° and 60°) and the curves calculated by using the soil parameters in Table 1, with respect to the relation among σ_1/σ_3 and (ε_1, ε_2 and ε_3). It can be estimated from these figures that the plane strain condition exists between θ=15° and θ=30°, because the intermediate principal strain ε_2 is expansive at θ=15° and is compressive at θ=30°.

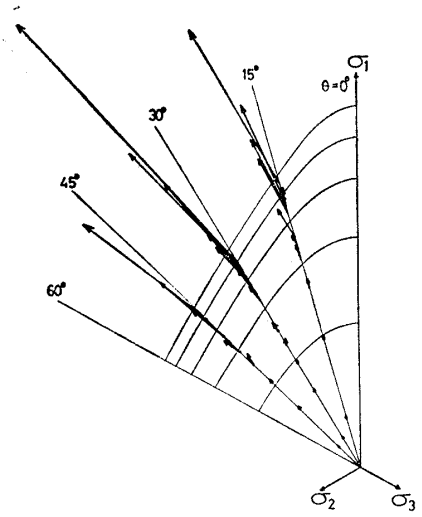

Fig. 24. Shear strain increment vectors on octahedral plane obtained by true triaxial test on sand

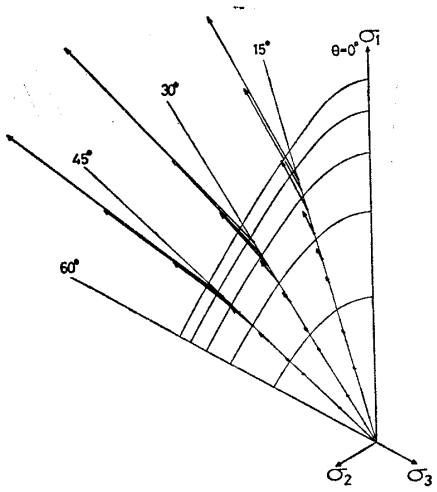

Fig. 25. Shear strain increment vectors on octahedral plane calculated by proposed model

This tendency also corresponds to that of other experimental results (Lade and Duncan, 1973).

Figs. 24 and 25 show the directions of projection of the strain increment vectors on the octahedral plane observed from the true triaxial tests ($\theta=15°, 30°$ and $45°$) and calculated by the proposed stress-strain model respectively. In these figures, the length of each vector is given by the ratio of the shear strain increment $d\gamma_{oct}$ to the shear-normal stress ratio increment $d(\tau_{oct}/\sigma_{oct})$. The calculated vectors in Fig. 25 explain well the test results shown in Fig. 24 that the directions of $d\gamma_{oct}$ deviate from those of τ_{oct} with a definite trend as the stress ratio increases. This tendency of the test results, however, was not explained by the former stress-strain model (Matsuoka and Nakai, 1974, 1977). Although the solid curves in these figures represent the criterion based on the SMP which is described below, both the observed and calculated vectors are not perpendicular to this criterion.

The authors have proposed the following failure criterion on the basis of the idea that soil fails when the shear-normal stress ratio on the SMP reaches a limiting value (Matsuoka and Nakai, 1974, 1977).

$$\frac{\tau_{SMP}}{\sigma_{SMP}}=\sqrt{\frac{J_1J_2-9J_3}{9J_3}}=\text{const.} \qquad (21)$$

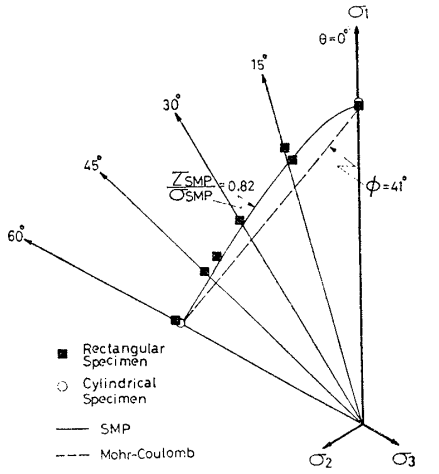

Fig. 26. Comparison of Mohr-Coulomb's and proposed criteria with stress conditions at failure on octahedral plane obtained by triaxial compression, triaxial extension and true triaxial tests on sand

or

$$\frac{J_1J_2}{J_3}=\text{const.} \qquad (22)$$

Fig. 26 compares the Mohr-Coulomb's and the proposed criteria with the stress conditions at failure on the octahedral plane obtained by the triaxial compression, triaxial extension and true triaxial tests on the sand. The stresses at failure in Fig. 26 mean the applied stresses when almost infinite strains are produced in the sand specimens. The test results

agree well with the proposed criterion illustrated by the solid curve. According to the proposed failure criterion, the internal friction angle ϕ has the same value under the triaxial compression and triaxial extension conditions, and has higher values under the three different principal stresses. Such characteristics of the strength of sand also correspond to the tendency of experimental results by Sutherland and Mesdary (1969).

Clay

Fig. 27 indicates the results of the triaxial compression and triaxial extension tests on the normally consolidated clay under the constant mean principal stress (σ_m=196 kN/m^2), with respect to the relation between τ_{SMP}/σ_{SMP} and $d\varepsilon_{SMP}^*/d\gamma_{SMP}^*$. Fig. 28 shows the results of the same tests with respect to the relation between τ_{SMP}/σ_{SMP} and $\varepsilon_{SMP}^*/\gamma_{SMP}^*$. It can be seen in these figures that the basic equations (Eqs. (11) and (12)) applied to the sand are also valid in the case of the clay. The soil parameters of the clay are determined as $\lambda^*=0.9$, $\mu^*=0.42$ and $\mu'^*=0.60$.

Fig. 29 shows the relation among τ_{SMP}/σ_{SMP}, γ_{SMP}^* and ε_{SMP}^* of the tests mentioned above, where the plots indicate the observed values and the solid curves the values calculated using Eqs. (14) and (15). By the way, in the case of the sand the soil paramenter γ_o^* varies depending on the mean principal stress as shown in Eq. (16), even if the initial soil structure is almost the same. However, in the case of the normally consolidated clay, the stress ratio-strain relationship under shear does not seem to be affected by the mean principal stress, as examined by the test results (Henkel, 1960; Shibata, 1963). Therefore, γ_o^* of the normally consolidated clay is considered to be independent of the mean principal stress, and determined as $\gamma_o^*=3.3\%$ ($\gamma_{oi}^*=3.3\%$, $C_d^*=0.0\%$). All of the soil parameters of the clay are shown in Table 2.

Figs. 30 and 31 show the results of the triaxial compression and extension tests on the clay with respect to the relation among the principal stress ratio (σ_1/σ_3), the major principal strain (ε_1) and the volumetric strain (ε_v), together with the curves calculated

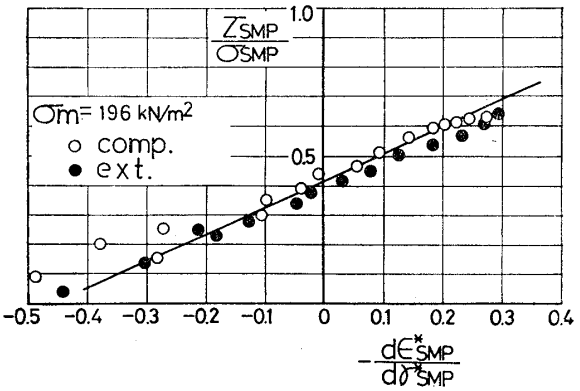

Fig. 27. Relation between τ_{SMP}/σ_{SMP} and $d\varepsilon_{SMP}^*/d\gamma_{SMP}^*$ obtained by triaxial compression and triaxial extension tests on clay

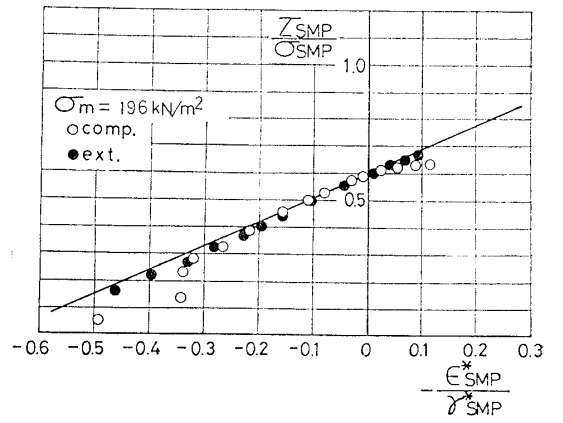

Fig. 28. Relation between τ_{SMP}/σ_{SMP} and $\varepsilon_{SMP}^*/\gamma_{SMP}^*$ obtained by same tests as Fig. 27

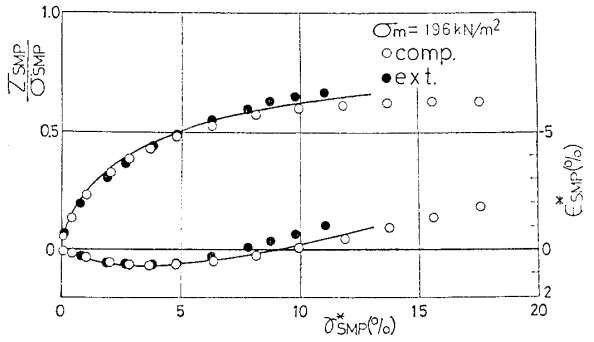

Fig. 29. Relation among τ_{SMP}/σ_{SMP}, γ_{SMP}^* and ε_{SMP}^* obtained by same tests as Fig. 27

Table 2. Values of all soil parameters for clay

λ^*		0.9
μ^*		0.42
μ'^*		0.60
γ_0^*	γ_{0i}^*	3.3%
	C_d^*	0.0%
	σ_{mi}	—

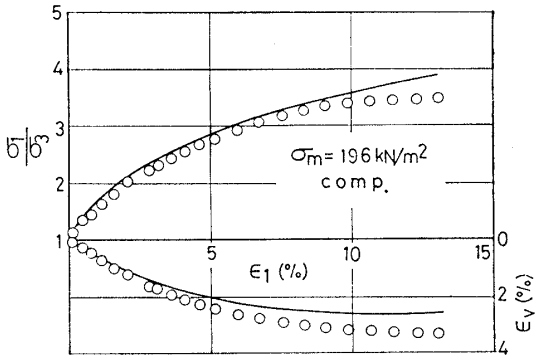

Fig. 30. Principal stress ratio vs. major principal strain vs. volumetric strain in triaxial compression test on clay

from Eqs. (14), (15) and (18). Although the true triaxial tests on the clay under three different principal stresses are not performed, it is considered that the proposed stress-strain model is valid for the clay as well as the sand since the deformation behaviors of the clay under both the triaxial compression and triaxial extension conditions can be analyzed by using the identical soil parameters in the same manner as those of the sand.

Now, according to the results of the current tests on the specimens without the slotted filter paper, the principal stress ratios at failure $(\sigma_1/\sigma_3)_f$ on the clay are almost 3.5 ($\phi \simeq 34°$) for both cases of the triaxial compression and triaxial extension conditions, as shown in Figs. 30 and 31. On the other hand, there have been some reports that the internal friction angle under the triaxial extension $\phi_{(ext.)}$ is larger than that under the triaxial compression $\phi_{(comp.)}$. The reason why $\phi_{(ext.)}$ is larger than $\phi_{(comp.)}$ might be considered that the effect of the tension of the slotted filter paper on the strength of clay is not negligible in the case of triaxial

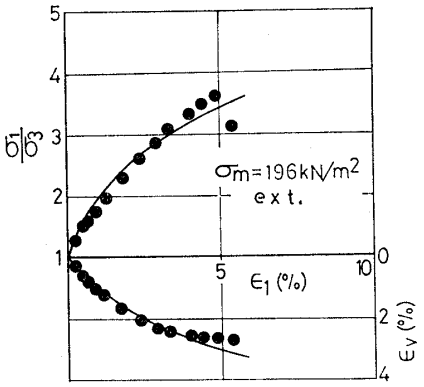

Fig. 31. Principal stress ratio vs. major principal strain vs. volumetric strain in triaxial extension test on clay

extension tests, even if the paper is put spirally.

CONCLUSIONS

The significance of the new concept based on the SMP (named SMP*) introduced in the current study is summarized as follows. For such granular materials as soils, it is necessary to determine the relations between the stress and the strain by connecting them with the average interparticle sliding. According to the present idea, the average interparticle sliding due to shear in the three-dimensional space is governed by the shear-normal stress ratio on the SMP (τ_{SMP}/σ_{SMP}), and the direction of the average interparticle sliding coincides with that of the principal strain increment vector. Therefore, it is reasonable that there exist the unique relations among τ_{SMP}/σ_{SMP} and the normal and parallel components of the principal strain increment vector to the SMP. Furthermore, it is interesting that the stress-strain relationship for such granular materials as soils is uniquely determined between the stress components which are given by the tensor transformation of the principal stresses as shown in Eqs. (4) and (5) and the strain increment components which are given by the vector transformation of the principal strain increments as shown in Eqs. (9) and (10).

The proposed stress-strain model does not

include the concept of a plastic potential function and a work-hardening function in the elastoplastic theory, but is derived fundamentally from the following two ideas. One is that the unique relations (Eqs. (11) and (12)) are present among τ_{SMP}/σ_{SMP}, $d\varepsilon_{SMP}^*$ and $d\gamma_{SMP}^*$ regardless of the stress condition. The other is that the direction of $d\gamma_{SMP}^*$ which represents the parallel component of the average interparticle sliding to the SMP is assumed to coincide with that of τ_{SMP}. It is checked by various kinds of shear tests including triaxial compression, triaxial extension and true triaxial tests that this stress-strain model can explain the deformation of sand and clay under the three-dimensional stress condition which have not been analyzed by the theories based on the octahedral plane and the former theory based on the SMP. For example, it is clear that this model can estimate properly the direction of strain increments in the three-dimensional space, from the facts that the relation between the stress ratio and strain increment ratio of Eq. (11) has a good estimate (see Figs. 8 and 9), and the calculated direction of $d\gamma_{oct}$ in Fig. 25 corresponds to the observed one in Fig. 24. It becomes evident that this model estimates properly the magnitude of strains under the three-dimensional stress condition, from the fact that Eqs. (14) and (15) hold regardless of the stress condition (see Figs. 17 to 19). Furthermore, the validity of the failure criterion based on the SMP which has been proposed is also examined by the various kinds of test data.

ACKNOWLEDGEMENTS

The authors wish to thank Professor T. Yamauchi at Nagoya Institute of Technology and Professor T. Shibata at Kyoto University for their helpful support and encouragement. They are also indebted to Messrs. H. Ishizaki, Y. Minami, S. Yokoi, Y. Nomura and Y. Suzuki for their experimental assistance and useful discussion. This study was undertaken by the financial support of Grant-in-Aid for Encouragement of Young Scientist, the Ministry of Education in Japan.

NOTATION

a_i $(i=1, 2, 3)$ = direction cosines of the normal of the SMP

b_i $(i=1, 2, 3)$ = direction cosines of τ_{SMP}

e_0 = initial void ratio

J_1, J_2, J_3 = first, second and third stress invariants

$d\gamma_{oct}$ = shear strain increment on the octahedral plane

$d\gamma_{SMP}$ = shear strain increment on the SMP

$d\gamma_{SMP}^*$ = parallel component of the principal strain increment vector to the SMP

$$\gamma_{SMP}^* = \int d\gamma_{SMP}^*$$

$d\varepsilon_1, d\varepsilon_2, d\varepsilon_3$ = major, intermediate and minor principal strain increments, respectively

$\varepsilon_1, \varepsilon_2, \varepsilon_3$, = major, intermediate and minor principal strains, respectively

ε_v = volumetric strain

$d\varepsilon_{oct}$ = normal strain increment on the octahedral plane

$d\varepsilon_{SMP}$ = normal strain increment on the SMP

$d\varepsilon_{SMP}^*$ = normal component of the principal strain increment vector to the SMP

$$\varepsilon_{SMP}^* = \int d\varepsilon_{SMP}^*$$

θ = angle of radial stress paths from σ_1 direction on the octahedral plane

$\lambda^*, \mu^* \mu'^*, \gamma_o^*$ = soil parameters in proposed stress-strain model

$\gamma_{oi}^*, C_d^*, \sigma_{mi}$ = coefficients related to γ_o^* (see Eq. (16))

M = soil parameter in Cambridge theory

$\sigma_1, \sigma_2, \sigma_3$ = major, intermediate and minor principal stresses, respectively

σ_m = mean principal stress

σ_{SMP} = normal stress on the SMP

τ_{SMP} = shear stress on the SMP

$X \equiv \tau_{SMP}/\sigma_{SMP}$ = shear-normal stress ratio on the SMP

ϕ = internal friction angle

ϕ_{moij} = mobilized angle between two principal stresses σ_i and σ (see

Fig. 2)

REFERENCES

1) Henkel, D. J. (1960) : "The relationship between the effective stress and water content in saturated clays," Géotechnique, Vol. 10, pp. 41-54.
2) Lade, P. V. and Duncan, J. M. (1973) : "Cubical triaxial tests on cohesionless soil," Proc., ASCE, Vol. 99, No. SM 10, pp. 793-812.
3) Matsuoka, H. (1974 a) : "A microscopic study on shear mechanism of granular materials," Soils and Foundations, Vol. 14, No. 1, pp. 29-43.
4) Matsuoka, H. (1974 b) : "Stress-Strain relationship of sands based on the mobilized plane," Soils and Foundations, Vol. 14, No. 2, pp. 47-61.
5) Matsuoka, H. and Nakai, T. (1974) : "Stress-deformation and strength characteristics of soil under three different principal stresses," Proc., JSCE, No. 232, pp. 59-70.
6) Matsuoka, H. and Nakai, T. (1977) : "Stress-strain relationship of soil based on the SMP," Proc., Specialty Session 9, 9 th ICSMFE, pp. 153-162.
7) Murayama, S. (1964) : "A theoretical consideration on a behaviour of sand," Proc., IUTAM Symposium on Rheology and Soil Mechanics, Grenoble, pp. 146-159.
8) Murayama, S. and Matsuoka, H. (1973) : "A microscopic study on shearing mechanism of soils," Proc., 8 th ICSMFE, Vol. 1, Part 2, pp. 293-298.
9) Nakai, T. and Matsuoka, H. (1980) : "A unified law for soil shear behaviour under three dimensional stress condition," Proc., JSCE, No. 303, pp. 65-77 (in Japanese).
10) Roscoe, K. H., Schofield, A. N. and Thurairajah, A. (1963) : "Yielding of clays in state wetter than critical," Géotechnique, Vol. 13, No. 3, pp. 211-240.
11) Shibata, T. (1963) : "On the volume change of normally-consolidated clays," Annuals, Disaster Prevention Research Institute, Kyoto University, No. 6, pp. 128-134 (in Japanese).
12) Schofield, A. N. and Wroth, C. P. (1968) : Critical State Soil Mechanics, Mcgraw-Hill, London.
13) Sutherland, H. B. and Mesdary, M. S. (1969) : "The influence of the intermediate principal stress on the strength of sand," Proc., 7 th ICSMFE, Vol. 1, pp. 391-399.

APPENDIX

It is proved as follows that the average sliding direction of the soil particles coincides with the direction of the principal strain increment vector under the three-dimensional stress condition: Fig. A1 shows a rectangular soil element of $L_1 \times L_2 \times L_3$ in length in the three-dimensional space where I, II and III axes represent the directions to which three principal stresses σ_1, σ_2 and σ_3 are applied, respectively. When the numbers of contact points of the sliding particles in the directions of I, II and III are n_1, n_2 and n_3, respectively, each incremental length caused by the interparticle sliding is given by the following formula as the summation of the sliding displacements at the interparticle contacts in each direction.

$$dL_1 = \sum_{i=1}^{n_1} (s_{i_1} \cdot \Delta l_i) \simeq n_1 \cdot \bar{s}_1 \cdot \overline{\Delta l}$$
$$dL_2 = \sum_{i=1}^{n_2} (s_{i_2} \cdot \Delta l_i) \simeq n_2 \cdot \bar{s}_2 \cdot \overline{\Delta l} \qquad \text{(A 1)}$$
$$dL_3 = \sum_{i=1}^{n_3} (s_{i_3} \cdot \Delta l_i) \simeq n_3 \cdot \bar{s}_3 \cdot \overline{\Delta l}$$

where, (s_{i1}, s_{i2}, s_{i3}) : direction cosines of the interparticle sliding at the contact point i.
Δl_i : sliding displacement at the contact point i.
$(\bar{s}_1, \bar{s}_2, \bar{s}_3)$: direction cosines of the average interparticle slid-

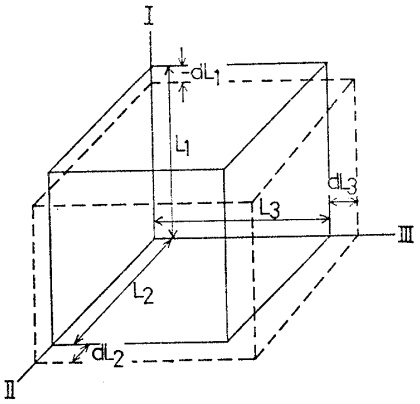

Fig. A 1. A rectangular soil element in three-dimensional space

ing.

$\overline{\Delta l}$: average sliding displacement at one contact point.

Then, if compressive strain is taken as positive sign, the principal strain increments are expressed as follows:

$$d\varepsilon_1=-\frac{dL_1}{L_1}=(n_1/L_1)\cdot\bar{s}_1\cdot\overline{\Delta l}$$

$$d\varepsilon_2=-\frac{dL_2}{L_2}=(n_2/L_2)\cdot\bar{s}_2\cdot\overline{\Delta l} \qquad \text{(A 2)}$$

$$d\varepsilon_3=-\frac{dL_3}{L_3}=(n_3/L_3)\cdot\bar{s}_3\cdot\overline{\Delta l}$$

On the assumption that the initial structure of soil is isotropic, the contact points of particles are considered to be uniformly distributed in the element. In such a case, the following relation holds, as the number of the contact points per unit length in every direction is equal.

$$\frac{n_1}{L_1}=\frac{n_2}{L_2}=\frac{n_3}{L_3} \qquad \text{(A 3)}$$

Therefore, the following equation is obtained from Eqs. (A 2) and (A 3).

$$\frac{d\varepsilon_1}{\bar{s}_1}=\frac{d\varepsilon_2}{\bar{s}_2}=\frac{d\varepsilon_3}{\bar{s}_3} \qquad \text{(A 4)}$$

Eq. (A 4) shows that the direction of the average interparticle sliding in the soil element corresponds with that of the principal strain increment vector.